Supporting Information

Studies of High-Membered Two-Dimensional Ruddlesden-Popper $Cs_7Pb_6I_{19}$ Perovskite Nanosheets via Kinetically Controlled Reactions

Yi-Chia Chen,[1] Kuan-Chang Wu,[1] Hsin-An Chen,[2] Wen-Hui Chu,[1] Swathi M. Gowdru,[1] Jou-Chun Lin,[1] Bi-Hsuan Lin,[3] Mau-Tsu Tang,[3] Chia-Che Chang,[1] Ying-Huang Lai,[1] Tsung-Rong Kuo,[4] Cheng-Yen Wen,[5] Di-Yan Wang[1]*

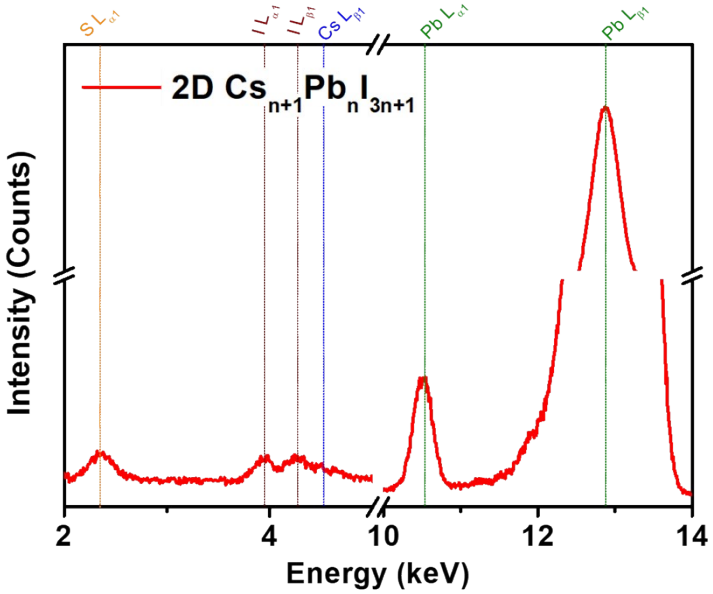

Figure S1. X-ray fluorescence spectra of 2D all-inorganic $Cs_{n+1}Pb_nI_{3n+1}$ perovskite nanosheets.

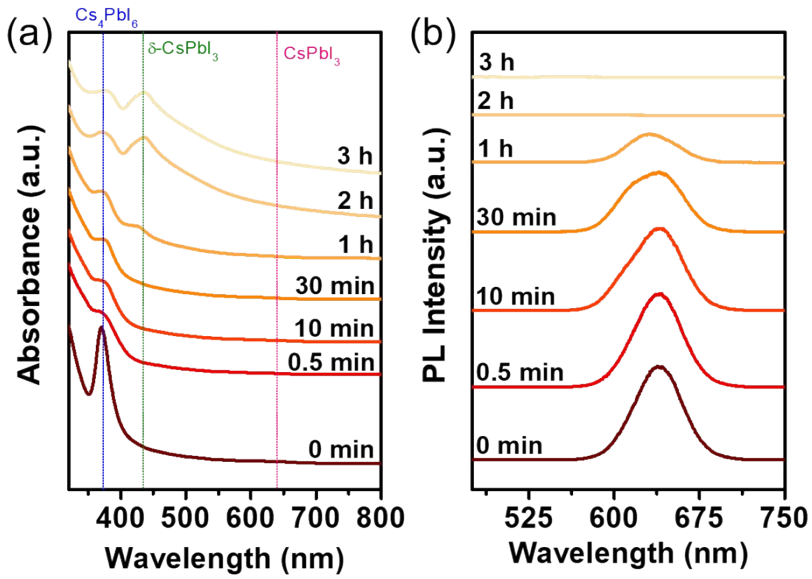

Figure S2. (a) in-situ absorption spectra and corresponding (b) in-situ PL spectra of 5 μL pristine $CsPbI_3$–Cs_4PbI_6 hybrid NCs solution diluted with 1 mL toluene for different dilution time.

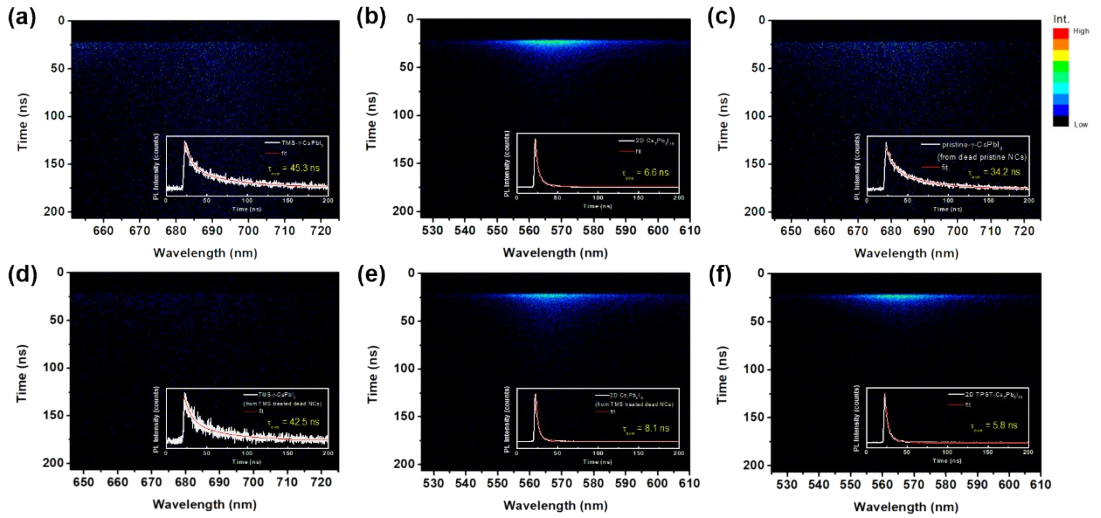

Figure S3. Streak camera images and corresponding time-resolved PL spectra with fitting results (inset) of (a) TMS-γ-$CsPbI_3$, (b) 2D $Cs_7Pb_6I_{19}$, (c) pristine-TMS-γ-$CsPbI_3$ formed from dead $CsPbI_3$−Cs_4PbI_6 hybrid NCs, (d) TMS-γ-$CsPbI_3$ formed from dead $CsPbI_3$−Cs_4PbI_6 hybrid NCs treated with TMS, (e) 2D $Cs_7Pb_6I_{19}$ formed from dead $CsPbI_3$−Cs_4PbI_6 hybrid NCs treated with TMS, and (f) 2D TPST-$Cs_7Pb_6I_{19}$ formed from a recrystallization process. (λ_{ex} = 375 nm). The TRPL decay curves were fitted by a biexponential decay function. The average lifetime obtained from (a) to (f) are 45.3 ns, 6.6 ns, 34.2 ns, 42.5 ns, 8.1 ns, and 5.8 ns, respectively.

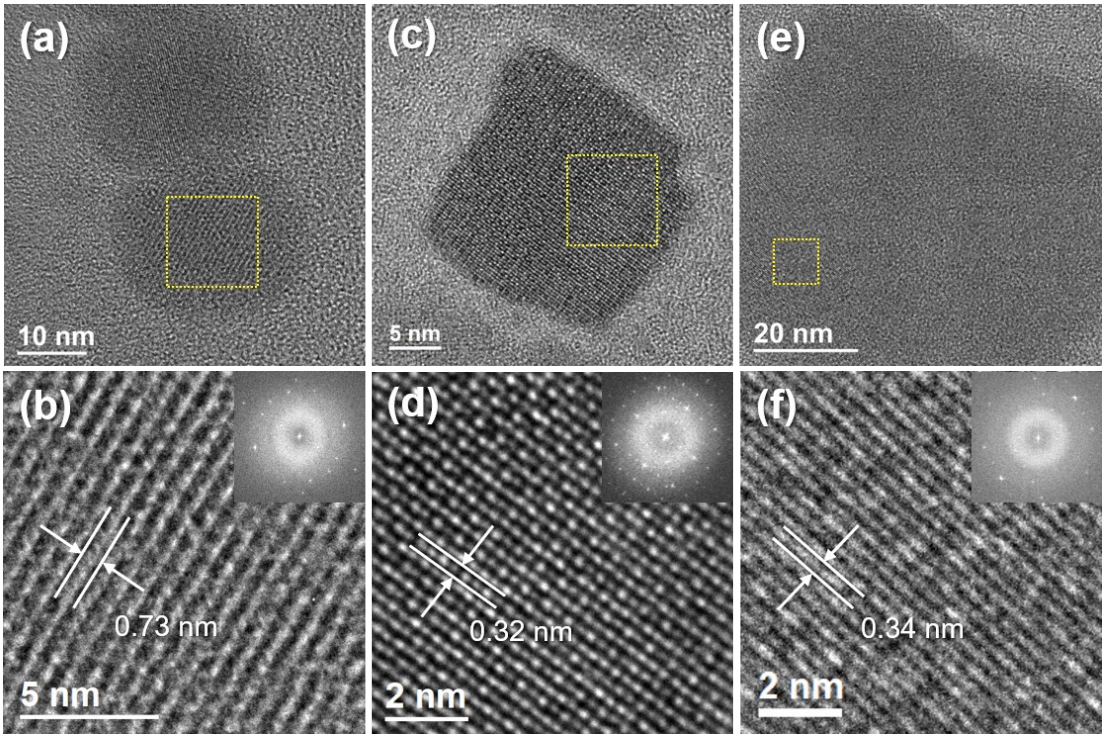

Figure S4. HRTEM images of (a-b) TMS treated $CsPbI_3$−Cs_4PbI_6 hybrid NCs before dilution. HRTEM images of (c-d) TMS-γ-$CsPbI_3$, and (e-f) 2D $Cs_7Pb_6I_{19}$ formed in the diluted concentration condition during a recrystallization process.

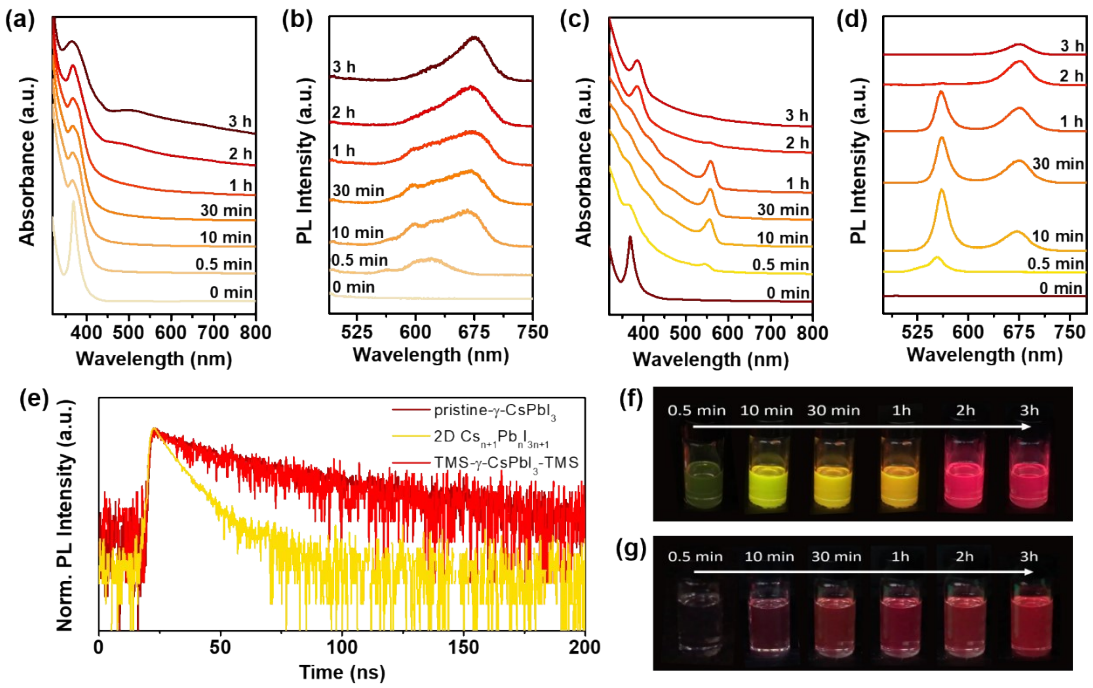

Figure S5. (a) In-situ absorption spectra and (b) in-situ PL spectra of **dead** $CsPbI_3$–Cs_4PbI_6 hybrid NCs diluted with toluene for different dilution time. (c) in-situ absorption spectra and corresponding (d) in-situ PL spectra of TMS treated dead $CsPbI_3$–Cs_4PbI_6 hybrid NCs diluted with toluene for different dilution time. (e) Time-resolved PL spectra of pristine-γ-$CsPbI_3$, 2D all-inorganic $Cs_{n+1}Pb_nI_{3n+1}$ perovskite and TMS-γ-$CsPbI_3$ that formed from dead $CsPbI_3$–Cs_4PbI_6 hybrid NCs were recorded by a streak camera at RT. (f) and (g) are the related photographs of TMS-treated and (e) non-TMS-treated dead $CsPbI_3$–Cs_4PbI_6 hybrid NCs diluted in toluene with emission color change for different reaction time.

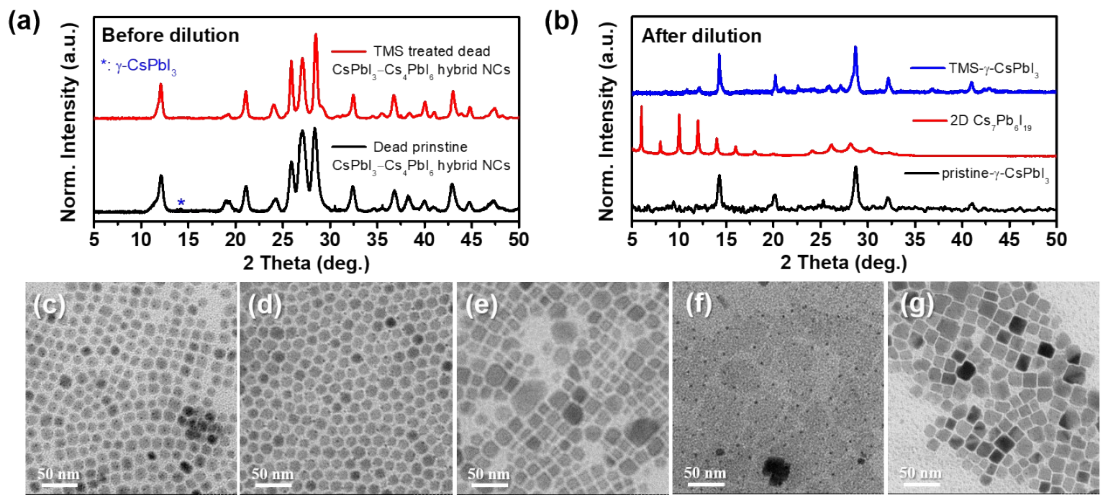

Figure S6. 2D all-inorganic $Cs_{n+1}Pb_nI_{3n+1}$ perovskite structure and 3D γ-phase $CsPbI_3$ formed from the perovkite solution with no optical activation, dead $CsPbI_3$–Cs_4PbI_6 hybrid NCs. (a) XRD patterns of dead pristine $CsPbI_3$–Cs_4PbI_6 hybrid NCs and that treated with TMS before dilution (b) XRD patterns of pristine-γ-$CsPbI_3$, 2D $Cs_7Pb_6I_{19}$, and TMS-γ-$CsPbI_3$ formed from dead $CsPbI_3$–Cs_4PbI_6 hybrid NCs in the diluted concentration condition during a recrystallization process. TEM images of (c) dead pristine $CsPbI_3$–Cs_4PbI_6 hybrid NCs and (d) that treated with TMS before dilution. TEM images of (e) pristine-γ-$CsPbI_3$, (f) 2D $Cs_7Pb_6I_{19}$ nanosheets, and (g) TMS-γ-$CsPbI_3$ formed from dead $CsPbI_3$–Cs_4PbI_6 hybrid NCs by a recrystallization process

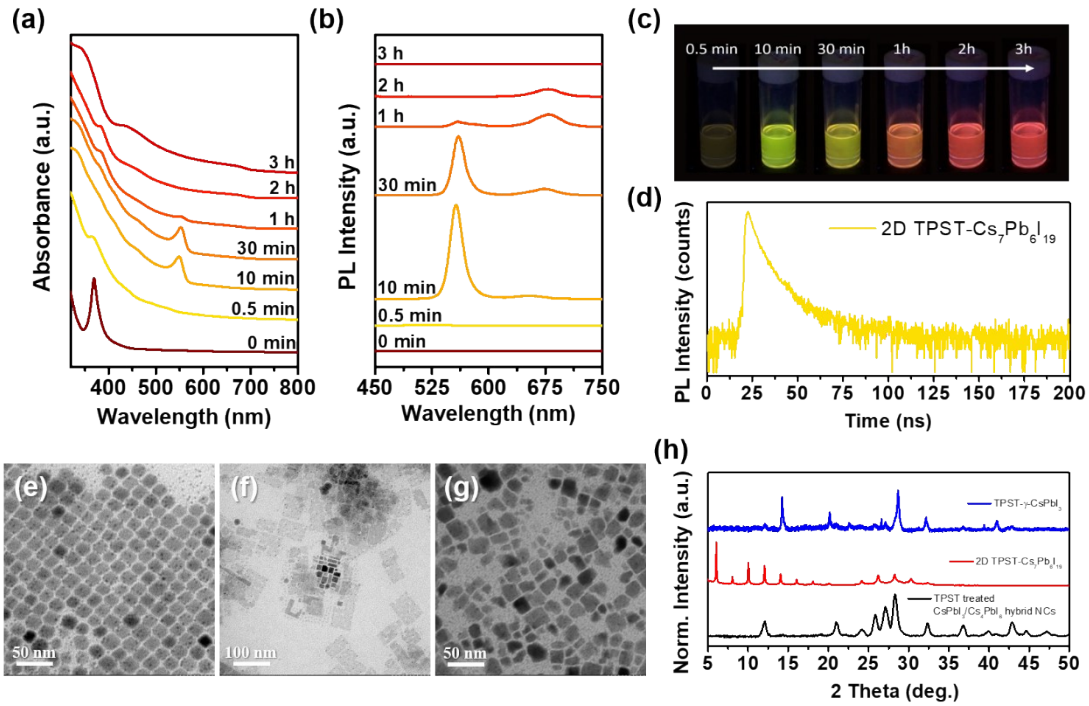

Figure S7. (a) In-situ absorption spectra and corresponding (d) in-situ PL spectra of **TPST** treated $CsPbI_3$–Cs_4PbI_6 hybrid NCs diluted with toluene for different dilution time. (c) Photographs of TPST-treated samples diluted in toluene with emission color change for different reaction time. (d) TRPL spectra of 2D TPST-$Cs_7Pb_6I_{19}$. TEM images of (e) undiluted TPST treated $CsPbI_3$–Cs_4PbI_6 hybrid NCs, (f) 2D TPST-$Cs_7Pb_6I_{19}$, and (g) TPST-γ-$CsPbI_3$. (h) XRD patterns of undiluted TPST treated $CsPbI_3$–Cs_4PbI_6 hybrid NCs, 2D TPST-$Cs_7Pb_6I_{19}$, and TPST-γ-$CsPbI_3$.

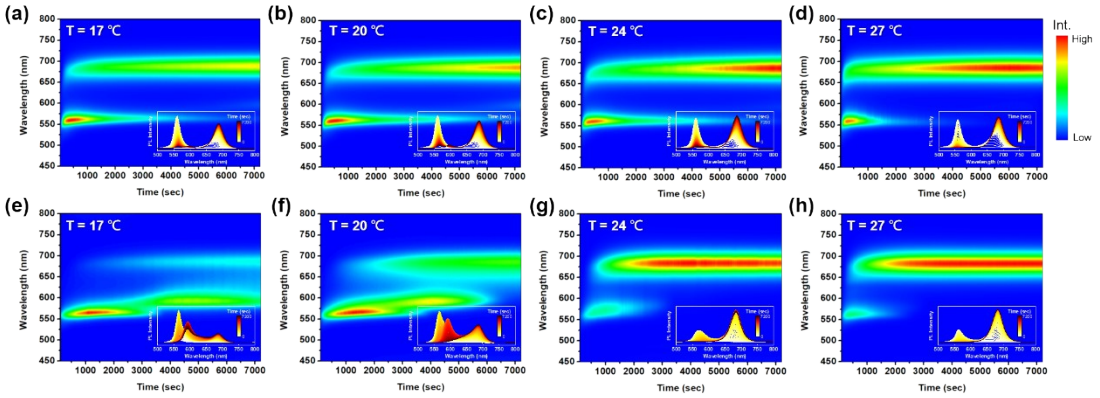

Figure S8. Two-dimensional (2D) contour map of time-dependent PL spectra acquired from the inset in-situ PL spectra under 17 °C, 20 °C, 24 °C, and 27 °C for (a-d) TMS treated $CsPbI_3$–Cs_4PbI_6 hybrid NCs and (e-h) TPST treated $CsPbI_3$–Cs_4PbI_6 hybrid NCs diluted with toluene solvent, respectively. (λ_{ex} = 430 nm)

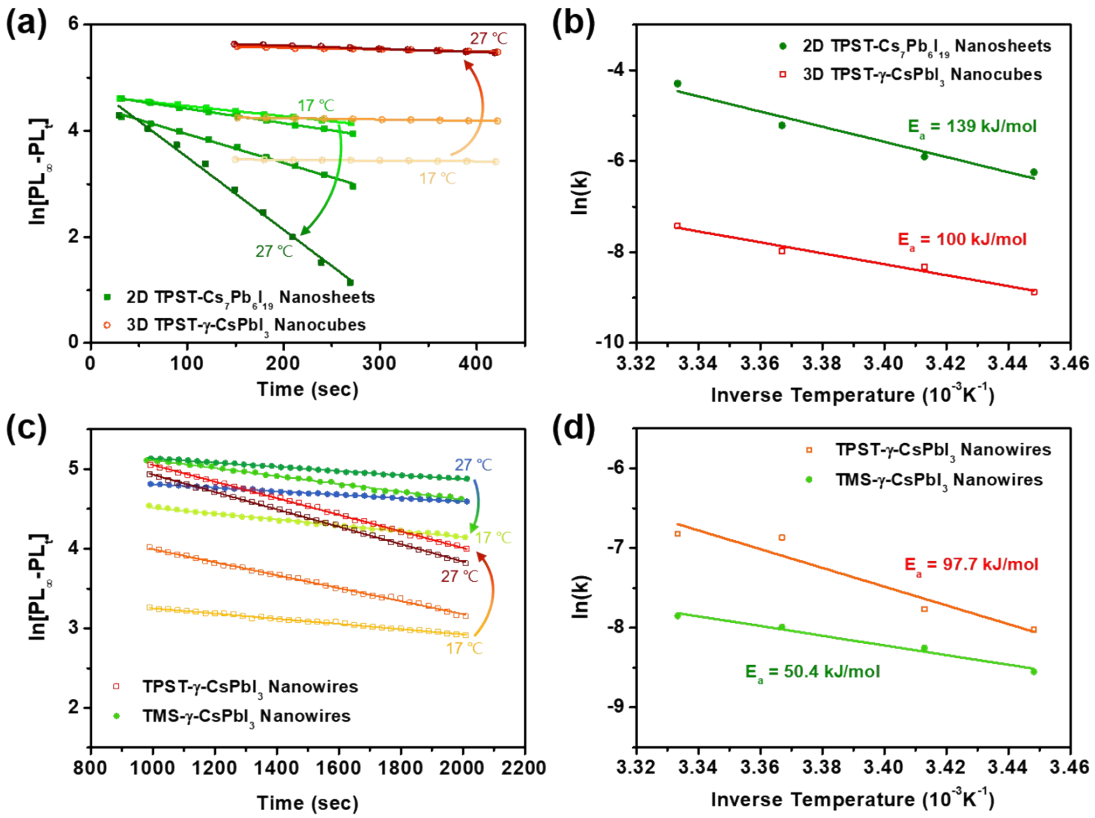

Figure S9. (a) The plots of the natural logarithm of $[PL_\infty - PL_t]$ as a function of time for the formation of 2D TPST-$Cs_7Pb_6I_{19}$ nanosheets and 3D TPST-γ-$CsPbI_3$ nanocubes at 17 °C, 20 °C, 24 °C, and 27 °C. (b) The Arrhenius plot fits of *ln* k against 1/T to obtained the activation energy of 2D TPST-$Cs_7Pb_6I_{19}$ nanosheets and 3D TPST-γ-$CsPbI_3$ nanocubes. (c) The plots of the natural logarithm of $[PL_\infty - PL_t]$ as a function of time for the formation of TMS-γ-$CsPbI_3$ nanowires and TPST-γ-$CsPbI_3$ nanowires at 17 °C, 20 °C, 24 °C, and 27 °C. (d) The Arrhenius plot fits of *ln* k against 1/T to obtained the activation energy of TMS-γ-$CsPbI_3$ nanowires and TPST-γ-$CsPbI_3$ nanowires.

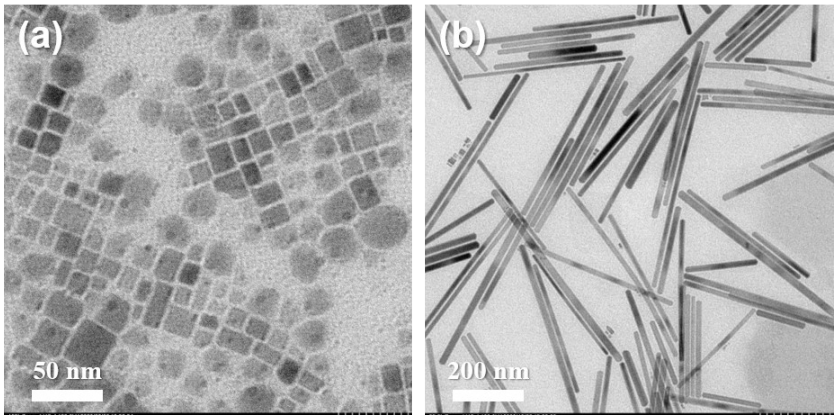

Figure S10. TEM images of different TMS-γ-$CsPbI_3$ structures in the two reaction steps of (a) within 500 seconds and (b) after 500 seconds that formed in diluted concentration conditions during a recrystallization process.

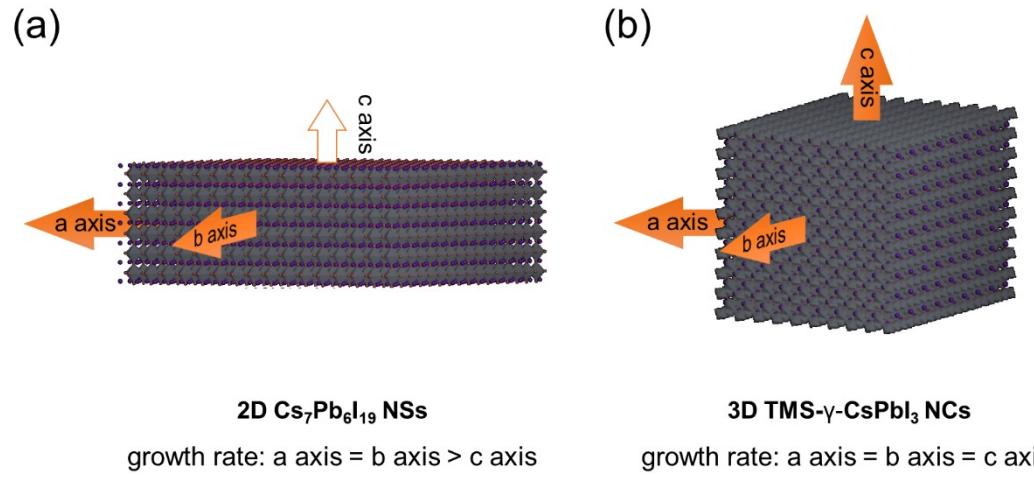

Figure S11. The schematic illustration of crystal growth mechanism of 2D $Cs_7Pb_6I_{19}$ NSs and 3D TMS-γ-$CsPbI_3$ NCs. The crystal structure grows along the a-axis and b-axis but not along the c-axis, which may be inhibited by TMS molecules, resulting in a higher formation rate of 2D $Cs_7Pb_6I_{19}$ than 3D TMS-γ-$CsPbI_3$ NCs.

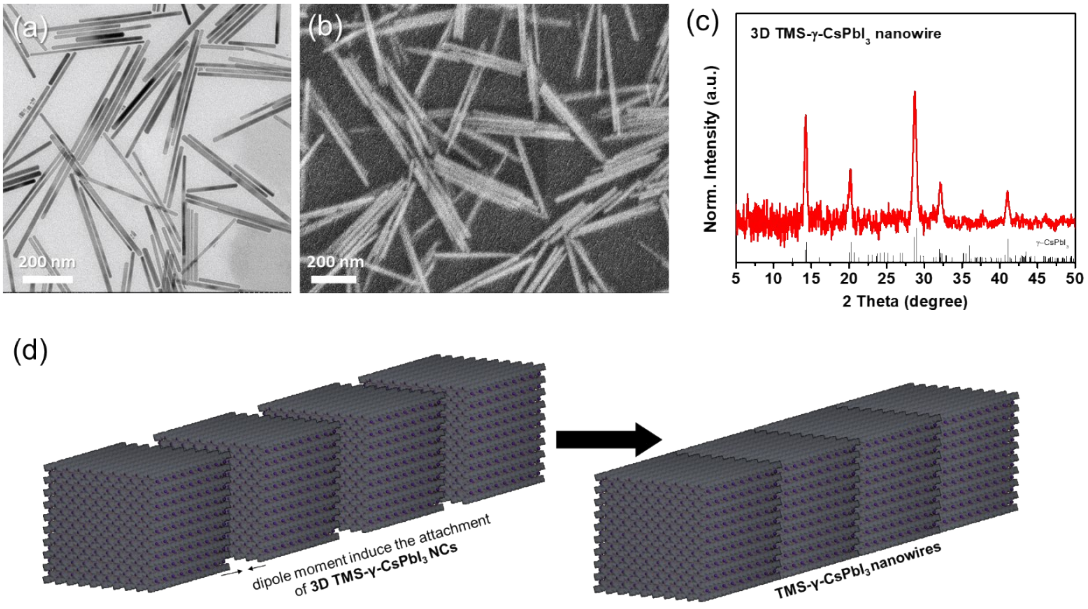

Figure S12. (a) TEM, (b) SEM images and (c) XRD pattern of 3D TMS-γ-$CsPbI_3$ nanowires. (d) The schematic illustration of phase evolution from 3D TMS-γ-$CsPbI_3$ NCs to 3D TMS-γ-$CsPbI_3$ nanowires.

According to the results of TEM, SEM images and XRD pattern (**Figure S12 (a)** to **(c)**, respectively), the perovskite nanowire is gamma structured. According to the images, the wire is indeed solid, not hollow. Although the formation rate of 3D TMS-γ-$CsPbI_3$ NCs is much slower than that of 2D RP $Cs_7Pb_6I_{19}$, we suggest that a few TMS molecules play an important

role in the structural evolution from nanocrystals to nanowires when 3D TMS-γ-$CsPbI_3$ NCs are formed. In the literature[1], the polar solvent molecules can induce the lattice distortion of ligand-stabilized cubic $CsPbI_3$ NCs, leading to the phase transition into orthorhombic phase. Such lattice distortion triggers the dipole moment on $CsPbI_3$ NCs, which subsequently initiates the hierarchical self-assembly of $CsPbI_3$ NCs into single-crystalline nanowires. In our case, the 3D TMS-γ-$CsPbI_3$ NCs have a cubic structure surrounded by residual TMS molecules that will induce their lattice distortion and increase the dipole moment, leading to the self-assembly of these nanocrystals (**Figure S12 (d)**). After that, the polarization of 3D TMS-γ-$CsPbI_3$ NCs is increased, resulting in its further distortion and peel off of amine ligands. Once the NCs get attached, they will fuse together and transform to γ-$CsPbI_3$ nanowire.

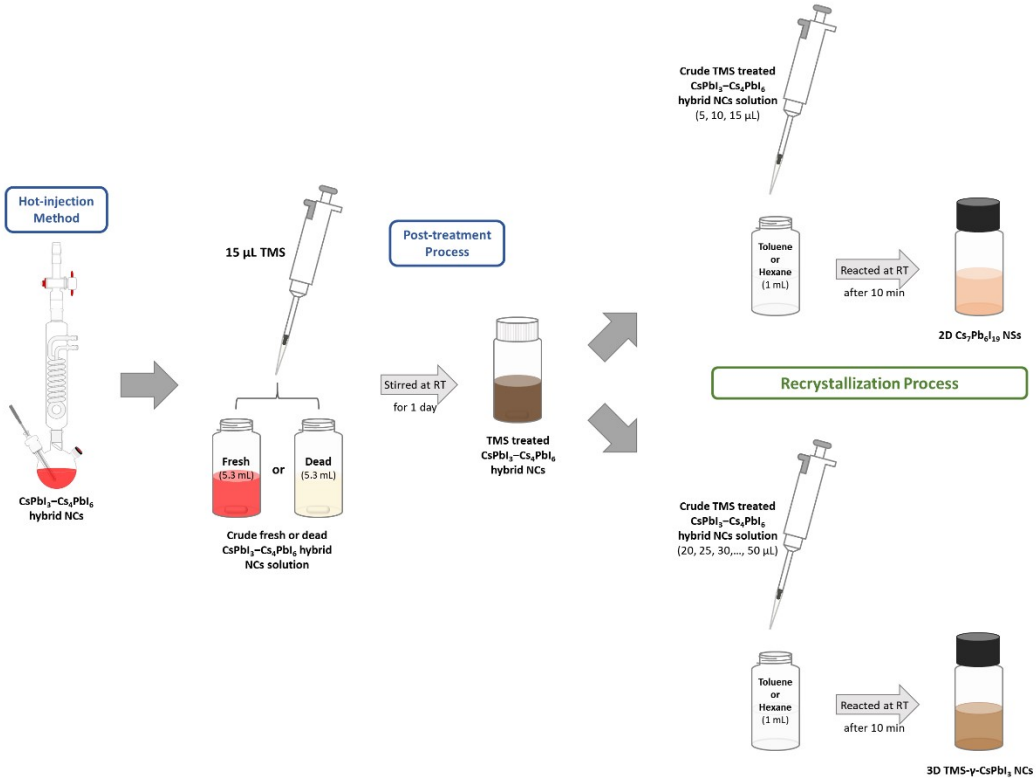

Figure S13. A flow chart of synthesis of 2D all inorganic RP perovskites. The 2D $Cs_7Pb_6I_{19}$ nanosheets were formed from the post-treated $CsPbI_3$–Cs_4PbI_6 hybrid perovskite nanocrystals at room temperature. The formation conditions of 2D $Cs_7Pb_6I_{19}$ nanosheets are as follows. 5, 10 and 15 µL of the crude post-treated $CsPbI_3$–Cs_4PbI_6 hybrid NCs solution was diluted and mixed with 1 mL of toluene or hexane to form the nucleated seed (the calculated concentration of Cs atom in the solution is ~0.045, 0.090 and 0.134 mM, respectively). The 2D $Cs_7Pb_6I_{19}$ perovskite nanosheets with green-yellow emission (at the Cs concentration from 0.045 to 0.134 mM) would be formed after 10 min.

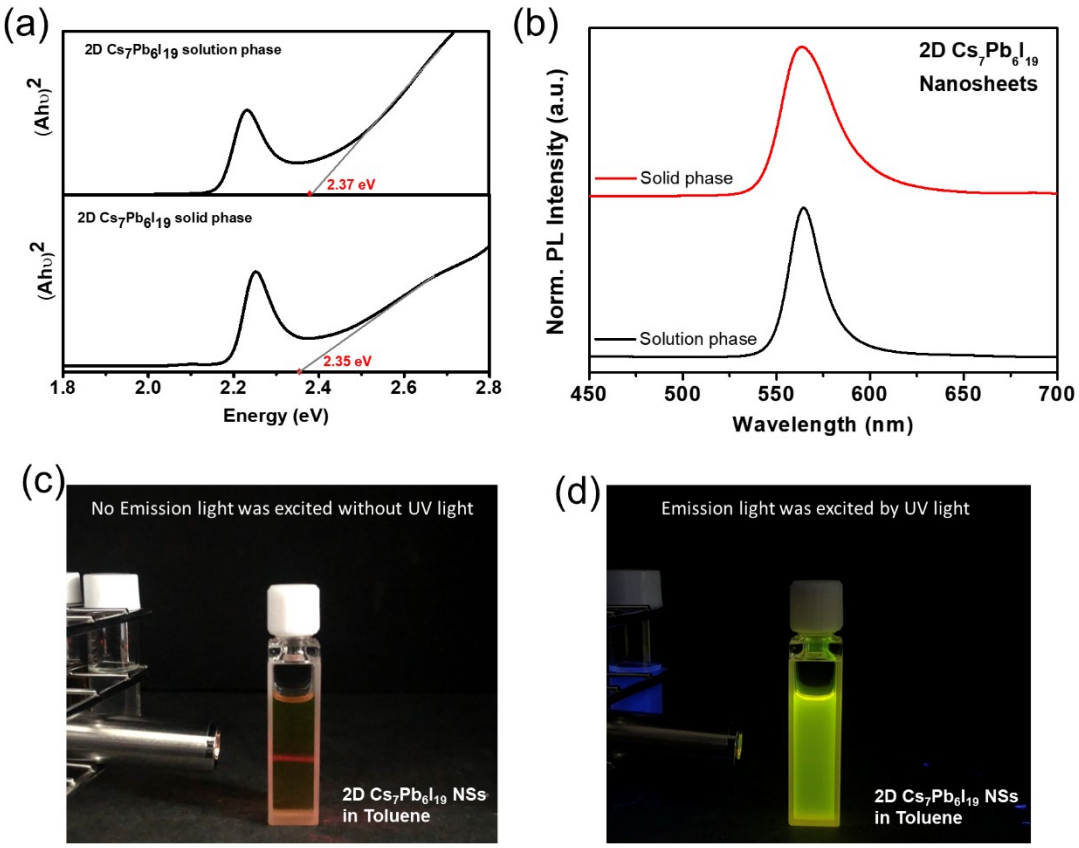

Figure S14. (a) The absorption spectra and (b) the PL spectra of 2D $Cs_7Pb_6I_{19}$ nanosheets in solution phase and solid phase. A Tyndall effect of 2D $Cs_7Pb_6I_{19}$ nanosheets in solution phase (c) without and (d) with UV light irradiation.

Figure S14 (a) and **(b)** show the absorption and PL spectra of 2D $Cs_7Pb_6I_{19}$ nanosheets in solution phase and solid phase, respectively. The band gaps of 2D $Cs_7Pb_6I_{19}$ NSs in solution (2.37 eV) and solid phase (2.35 eV) were estimated similarly by the Tauc plot method. Besides, we also found that the PL emission of 2D $Cs_7Pb_6I_{19}$ in solid phase is very similar to that in solution. The FWHM of PL spectra of solid phase exhibited a little larger than that of solution phase. It could be attributed to the fact that more surface defects of 2D $Cs_7Pb_6I_{19}$ in the solid phase are increased by the leakage of surfactant during the drying process from solution to solid phase. Therefore, we suggest that PL emission spectra originate from the formation of 2D $Cs_7Pb_6I_{19}$ nanosheets. **Figure S14 (c)** and **(d)** show a Tyndall effect of 2D $Cs_7Pb_6I_{19}$ nanosheets in the solution phase. This is a common phenomenon found in the solution phase of perovskite nanocrystals.[2] The Tyndall effect is a light-scattering effect caused by suspended colloids as a light beam passes through a colloidal solution, which makes the light beam visible in the colloidal solution. The amount of scattering depends on the size and density of the colloids. Therefore, the size of 2D $Cs_7Pb_6I_{19}$ nanosheets is around several hundred nanometers, resulting in an obvious Tyndall effect in the solution phase. Considering the measurement of PL spectra affected by the Tyndall effect, there are two methods to prevent scattering light from this effect, resulting in measuring the correct optical spectrum in the solution phase. First, because the

detector of PL spectroscopy is perpendicular to the exciting light source, very little scattered light will be detected by the detector. Second, the scattering light comes mainly from exciting light, which will be filtered out from the filter. Therefore, the optical properties of 2D $Cs_7Pb_6I_{19}$ nanosheets can be revealed from the measurement of PL spectra.

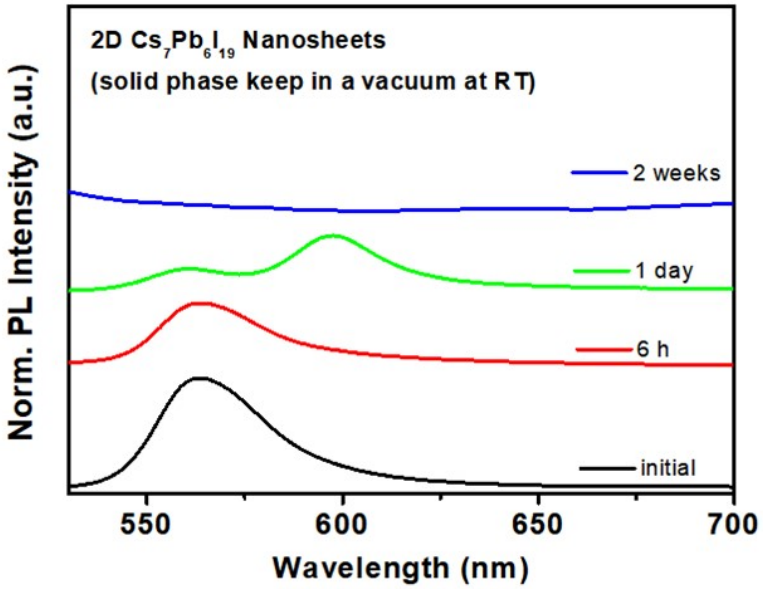

Figure S15. The PL spectra of the solid phase 2D $Cs_7Pb_6I_{19}$ nanosheets were stored in vacuum at room temperature for 6 h, 1 day, and 2 weeks. The results showed the PL emission of the 2D $Cs_7Pb_6I_{19}$ (560 nm) was gradually decayed in several days under vacuum at room temperature. However, it exhibited more optical stability compared to the solution phase. The emission of 2D $Cs_7Pb_6I_{19}$ (560 nm) in toluene solution phase would be present for only one hour, but can still be observed in the solid state for 24 hours. One emission peak around 600 nm appeared for one day, indicating the possibility of the 2D perovskite aggregation into 3D or 3D $CsPbI_3$ nanomaterial formation. More details of the solid phase transition mechanism will be investigated in the future work.

To investigate the stability of 2D $Cs_7Pb_6I_{19}$ under annealing condition, the emission photograph of 2D $Cs_7Pb_6I_{19}$ coated on the slide glass was performed at 100 °C. In **Figure S16 (a)**, We found that the yellow emission color of 2D $Cs_7Pb_6I_{19}$ quickly changed to red and then no light was emitted, indicating that it exhibits poor thermal stability at high temperatures. After a thermal annealing process of 80 min, the XRD spectra showed that the crystal structure of 2D $Cs_7Pb_6I_{19}$ was changed to δ-$CsPbI_3$, as shown in **Figure S16 (b).**

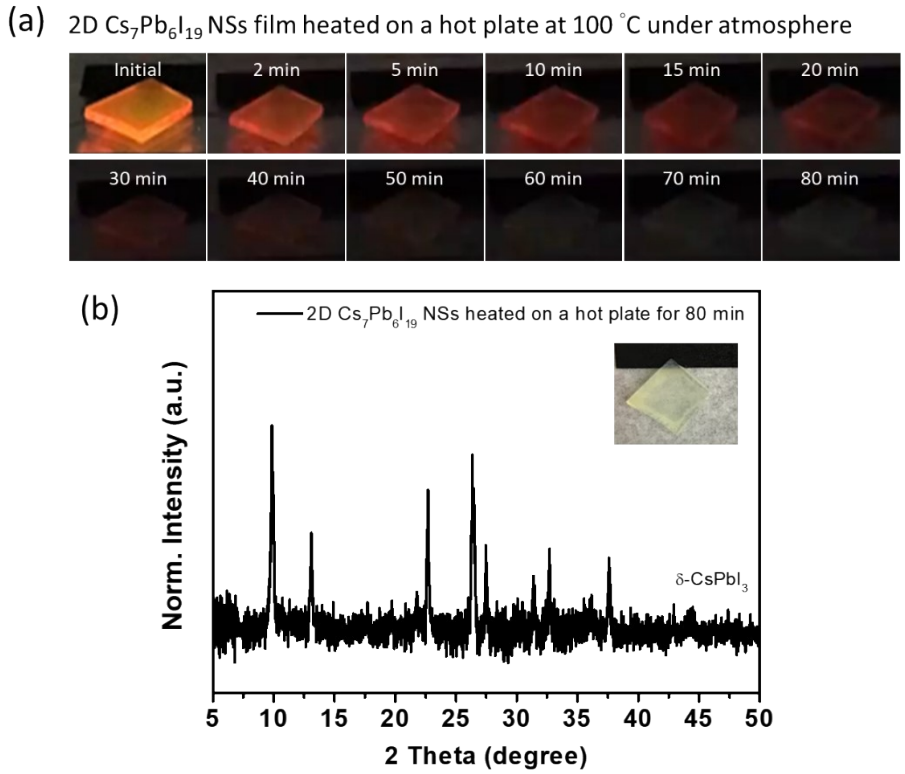

Figure S16. (a) The photographs of 2D $Cs_7Pb_6I_{19}$ nanosheets film were heated on a hot plate under the atmosphere for different times with a UV light irradiation (365 nm). (b) The XRD pattern of the 2D $Cs_7Pb_6I_{19}$ film, which was heated on a hot plate under the atmosphere for 80 min. The inset is the corresponding photograph of the film under white light.

Table S1. Calculation results of chemical kinetics for 2D $Cs_7Pb_6I_{19}$ and 3D γ-$CsPbI_3$ that formed from TMS or TPST treated samples by using a recrystallization process at four temperatures. The average formation or decay rate constants were obtained by the rate law of first-order reaction.

	2D $Cs_7Pb_6I_{19}$ NSs (formation)		**2D $Cs_7Pb_6I_{19}$ NSs (decay)**		**3D TMS-γ-$CsPbI_3$ NCs (formation)**		**TMS-γ-$CsPbI_3$ NWs (formation)**	
Temp. (°C)	k (s^{-1})	E_a (kJ/mol)	k (s^{-1})	E_a (kJ/mol)	k (s^{-1})	E_a (kJ/mol)	k (s^{-1})	E_a (kJ/mol)
17	1.82×10^{-3}	151	2.38×10^{-4}	75.5	6.59×10^{-4}	95.3	1.93×10^{-4}	50.4
20	3.64×10^{-3}		2.87×10^{-4}		1.11×10^{-3}		2.61×10^{-4}	
24	8.29×10^{-3}		5.45×10^{-4}		1.55×10^{-3}		3.39×10^{-4}	
27	1.48×10^{-2}		6.17×10^{-4}		2.66×10^{-3}		3.90×10^{-4}	
	2D TPST-$Cs_7Pb_6I_{19}$ NSs (formation)		**2D TPST-$Cs_7Pb_6I_{19}$ NSs (decay)**		**3D TPST-γ-$CsPbI_3$ NCs (formation)**		**TPST-γ-$CsPbI_3$ NWs (formation)**	
Temp. (°C)	k (s^{-1})	E_a (kJ/mol)	k (s^{-1})	E_a (kJ/mol)	k (s^{-1})	E_a (kJ/mol)	k (s^{-1})	E_a (kJ/mol)
17	1.94×10^{-3}	139	4.76×10^{-4}	84	1.39×10^{-4}	100	3.27×10^{-4}	97.7
20	2.73×10^{-3}		6.59×10^{-4}		2.41×10^{-4}		4.24×10^{-4}	
24	5.43×10^{-3}		8.62×10^{-4}		3.44×10^{-4}		1.04×10^{-3}	
27	1.37×10^{-2}		1.65×10^{-3}		6.01×10^{-4}		1.09×10^{-3}	

To investigate the relative thermodynamic stability of 2D RP $Cs_7Pb_6I_{19}$, we performed density functional theory (DFT) calculations. The detailed crystallographic information of 2D $Cs_7Pb_6I_{19}$ was provided as follows. 2D $Cs_7Pb_6I_{19}$ crystallizes in the tetragonal space group of I4/mmm with unit cell parameters of a = b = 6.3054 Å, c = 89.0813 Å, α = 90°, β = 90°, and γ = 90°. Detailed crystallographic data and atomic parameters of 2D $Cs_7Pb_6I_{19}$ are shown in **Table S2** and **S3**, respectively. The crystal system of 2D $Cs_7Pb_6I_{19}$ (tetragonal) is the same as that of $Cs_2PbI_2Cl_2$ [3] or Cs_2PbI_4 [4].

Table S2. Crystallographic data for 2D $Cs_7Pb_6I_{19}$.

Compound	**n = 6**
Formula Sum	$Cs_{14}Pb_{12}I_{38}$
Crystal System	Tetragonal
Space Group	I4/mmm
Cell Parameters	a = b = 6.3054 (Å) c = 89.0813 (Å) α = 90° β = 90°

	γ = 90°
	a/b = 1.0000
Cell Ratio	b/c = 0.0708
	c/a = 14.1278
Cell Volume	3541.70 Å^3

Table S3. Atomic parameters for 2D $Cs_7Pb_6I_{19}$.

Atom	x/a	y/b	z/c	U [Å^2]
Cs1	1/2	1/2	0.79551	0.0000
Cs7	1/2	1/2	0.86104	0.0000
I1	1/2	1/2	0.28682	0.0000
Pb3	1/2	1/2	0.39386	0.0000
Pb7	1/2	1/2	0.32188	0.0000
Cs2	1/2	1/2	0	0.0000
Cs4	0	0	0.43018	0.0000
I7	0	0	0.14133	0.0000
I17	0	0	0.92958	0.0000
Pb1	0	0	0.03507	0.0000
I2	0	1/2	0.96519	0.0000
I9	0	1/2	0.17473	0.0000
I3	1/2	0	0.60462	0.0000
I6	1/2	1/2	1/2	0.0000

Table S4. Crystallographic data for γ-$CsPbI_3$ and δ-$CsPbI_3$.[5]

	Crystal System	Space Group	Z	a	b	c	Volume (Å^3)
γ-$CsPbI_3$	orthorhombic	Pnma	4	8.8637(8)	12.4838(12)	8.5783(8)	949.21(15)
δ-$CsPbI_3$	orthorhombic	Pnma	4	10.4500(5)	4.7965(2)	17.7602(8)	890.20(7)

The calculated formation energy of δ-$CsPbI_3$, γ-$CsPbI_3$ and 2D $Cs_7Pb_6I_{19}$

In comparing the formation energy among δ-$CsPbI_3$, γ-$CsPbI_3$ and 2D $Cs_7Pb_6I_{19}$, a batch of ab-initio simulations was employed. Geometry optimizations and single point energy calculations were performed by using the Vienna Ab initio Simulation Package (VASP). The generalized gradient approximation was used with the Perdew-Burke-Ernzerh (PBE) of exchange-correlation functional and the projector-augmented wave pseudopotentials in all calculations. The cutoff energy was set to 400 eV, and k-point meshes with k-spacing of 0.250 ($Å^{-1}$) and 0.125 ($Å^{-1}$) were used in geometry optimizations and single point energy calculations, respectively. The self-consistent field convergence criterion for optimization was set to $\Delta E < 10^{-6}$ eV. The DFT-D3 correction was considered in all calculations in incorporating the van der Waals interactions between atoms. The formation energy was calculated from the following equation, $E_f(Cs_aPb_bI_c) = E(Cs_aPb_bI_c) - aE(Cs) - bE(Pb) - cE(I)$, where $E(Cs)$, $E(Pb)$ and $E(I)$ are the atomic energies according to the respective bulk structures.

The results showed that the formation energy of RP (-1.095 eV) is higher than that of gamma (-1.106eV) /delta (-1.121 eV) phases. The value of gamma and delta phase is closer to Materials project (open source). Moreover, the changed trend is similar to the literature report[6], which indicated that the formation energy of 2D $Cs_7Pb_6I_{19}$ is higher than that of 3D structure.

Reference

1. J.-K. Sun, S. Huang, X.-Z. Liu, Q. Xu, Q.-H. Zhang, W.-J. Jiang, D.-J. Xue, J.-C. Xu, J.-Y. Ma, J. Ding, Q.-Q. Ge, L. Gu, X.-H. Fang, H.-Z. Zhong, J.-S. Hu and L.-J. Wan, *J. Am. Chem. Soc.*, 2018, **140**, 11705-11715.
2. W. Zheng, P. Huang, Z. Gong, D. Tu, J. Xu, Q. Zou, R. Li, W. You, J.-C. G. Bünzli and X. Chen, *Nat. Commun.*, 2018, **9**, 3462.
3. J. Li, Q. Yu, Y. He, C. C. Stoumpos, G. Niu, G. G. Trimarchi, H. Guo, G. Dong, D. Wang, L. Wang and M. G. Kanatzidis, *J. Am. Chem. Soc.*, 2018, **140**, 11085-11090.
4. Y.-F. Ding, Q.-Q. Zhao, Z.-L. Yu, Y.-Q. Zhao, B. Liu, P.-B. He, H. Zhou, K. Li, S.-F. Yin and M.-Q. Cai, *J. Mater. Chem. C*, 2019, **7**, 7433-7441.
5. D. B. Straus, S. Guo and R. J. Cava, *J. Am. Chem. Soc.*, 2019, **141**, 11435-11439.
6. A. Bala, A. K. Deb and V. Kumar, *J. Phys. Chem. C*, 2018, **122**, 7464-7473.